Multi-parametric space-time computational vademecum for parametric studies: Application to real time welding simulations

Ye Lu, Nawfal Blal, Anthony Gravouil

Multi-parametric space-time *computational vademecum* for parametric studies: Application to real time welding simulations

Ye Lu[a,b], Nawfal Blal[a], Anthony Gravouil[a,*]

a Univ Lyon, INSA-Lyon, CNRS UMR5259, LaMCoS, F-69621, France

b Chaire AREVA-SAFRAN, INSA, France

Real time simulations of welding processes remain intractable despite the impressive increasing computing power. This paper presents the case of a thermo-elasto-plastic problem with located moving heat loading. A novel non-intrusive *a posteriori* reduced order strategy for building multiparametric *computational vademecum* dedicated to real-time simulations of nonlinear thermo-mechanical problems is proposed. The high order proper generalized decomposition (HOPGD) is used to seek separated representation of solutions with some precom-puted snapshots. Furthermore, a relaxation method is successfully applied to accelerate this procedure. The accuracy of the constructed *computational vademecum* is controlled by a localized multigrid selection method that allows an automatic selection of snapshots in the areas of interest of the parameter space. Examples of multiparametric *computational vademecum* taking into account some material parameters will be shown in this paper.

1. Introduction

In spite of the impressive progresses in computer science, traditional approaches reach some limitations when dealing with nonlinear parametric problems, like in inverse identification or optimization of the welding or additive manufacturing processes. A very large number of solutions of the concerned model has to be computed for different values of the problem parameters. In addition, when real-time simulations are required, it remains intractable with traditional computational approaches, due to the increasing degrees of freedom and complexity of the models.

In this context, model order reduction (MOR) techniques [1] have been developed recently. The resulting *computational vademecum* [2] (called also virtual charts [3,4] or meta-model computations), actually a series of parametric solutions, allows real-time simulations of parametric problems and open numerous possibilities in integrated simulation-based engineering. The construction of *computational vademecum* consists in usually two stages: offline and online. With the MOR techniques, the parametric solutions are computed and stored as a series of vectors (reduced bases) at offline stage once for all for building the *computational vademecum*. Then the *computational vademecum*, served as a sort of numerical or graphical handbook, can provide a real-time response for any value of parameters at the online phase. Depending on the way the reduced bases (RBs) are built with, two families of MOR approaches can be distinguished: *a posteriori* and *a priori*.

A posteriori approaches consist, usually, in employing the proper orthogonal decomposition (POD) method [5] to extract the most significant characteristic of the solution as RB that can be then applied to models with slight changes to the original one. Thus this kind of approaches needs some priori computed solutions and the resulting reduced order models can be usually solved efficiently. The POD-based MOR has been successfully applied in the context of solid mechanics (see e.g. Refs. [6–13]). The main issue of such approaches is the loss of efficiency when dealing with nonlinear problems with high parametric dependency. Several approaches, e.g. the Empirical Interpolation Method (and its discrete counterpart DEIM) [14,15], the hyper-reduction methods [9,16,17] and the asymptotic numerical method [5,18,19] that allows eliminating the re-computation of the tangent matrix, are introduced to accelerate the computations, but real time requirements remain intractable.

The other family of approaches, i.e. *a priori*, is based on the proper generalized decomposition (PGD) [20–22]. The main advantage of these approaches lies in the separated representations of solutions, which is firstly introduced under the name of “radial approximation” [23] by Pierre Ladeveze in the 80s within the framework of the LArge Time INcrements (LATIN) method [24,25], for solving high nonlin-

* Corresponding author.
E-mail addresses: Ye.Lu@insa-lyon.fr (Y. Lu), Nawfal.Blal@insa-lyon.fr (N. Blal), Anthony.Gravouil@insa-lyon.fr (A. Gravouil).

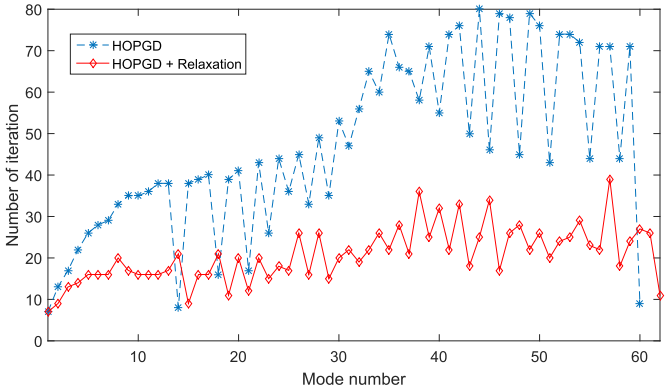

Fig. 1. Number of iterations during the construction of 3D PGD approximations.

Table 1
CPU time for 3D HOPGD.

	Number of modes	Iterations	CPU time
HOPGD	60	2832	400 s
HOPGD + Relaxation	62	1284	240 s

Table 2
CPU time of 5D HOPGD.

	Number of modes	Iterations	CPU time
HOPGD	91	4528	915 s
HOPGD + Relaxation	97	2641	563 s

ear problems. These PGD-based methods do not require any previous solution and the RBs are built on-the-fly by solving the resulting multi-dimensional models in which model parameters (boundary conditions, initial conditions, geometrical parameters, material and process parameters …) are considered as extra-coordinates. Many problems are solved using the PGD approaches; interested readers are referred to [20,21,26–29] and the references therein. A series of *computational vademecum* are constructed for different problems in sciences and engineering such as thermal control of industrial furnaces [30], shape optimization [2,4], computational surgery [31–33], etc. The use of *computational vademecum* can provide real-time responses at the online phase, since the multidimensional models have been solved offline for every possible value of parameters. This opens various possibilities and development in integrated simulation-based engineering. However, such approaches are usually intrusive. In particular, one can cite a recent paper [42] successfully using the PGD-based approach for the thermal process of welding, however, the application for nonlinear mechanical problems involving material plasticity is still under development.

For the sake of avoiding the intrusive aspect, recently, a POD-based *computational vademecum* [34] has been built through an *a posteriori* approach for welding processes. In this work, snapshots are computed with the standard finite element (FE) method. A manifold-based method [17,34,35] is proposed to interpolate both the space and time POD-RBs with respect to the variation of parameters. Thus there is no complex computation at the online phase (no equilibrium equations have to be solved) and real-time space-time responses can be obtained. This strategy of construction of *computational vademecum* without intrusive effects has been applied to standard welding simulations. The real-time *computational vademecum* can be helpful for engineers to make optimization decisions of welding processes.

In the same context, this paper presents an alternative *a posteriori* non-intrusive tool to build the multiparametric real time space-time *computational vademecum* using the high order PGD (HOPGD) method [36]. Similarly to PGD methods, the problem parameters are considered as extra-coordinates of solutions. Then a separated representation of solutions is constructed by HOPGD. However, the RB functions are computed offline, through an *a posteriori* approach, with some precomputed snapshots. The greedy algorithm incorporated with an alternative fixed point strategy is used for the search of the basis functions. In order to increase the convergence rate, the dynamic relaxation method (i.e. Aitken's Delta Squared method [37–39]) is proposed to accelerate the greedy algorithm. Its efficiency will be shown with several examples in this paper. Once the basis functions are constructed offline, solutions for new values of parameters can be provided online by the *computational vademecum* at real-time rates.

In order to control the accuracy of *computational vademecum*, a local refinement methodology [34] is applied to select the necessary snapshots in the parameter space for a given error. Exhaustive generations of snapshots, at expensive computational cost, can be then avoided.

Starting with the problem statement, this paper introduces the weakly coupled thermo-mechanical formulation in section 2. A new strategy with HOPGD method for building multiparametric *computational vademecum* is presented in section 3. The convergence accelerator of HOPGD will also be presented. Section 4 presents some application examples of the proposed approach. Finally, *computational vademecum* dedicated to parametric studies of welding processes will be shown at the end with a sensitivity analysis.

Notation: In this paper, the studied quantities of interest depend on the space-time coordinates $(\mathbf{X},t)\in\Omega\times[0,T]\subset\mathbb{R}^4$ and a set of parameters $\mu\in D\subset\mathbb{R}^d$. The associated physical problem is then said to be a $(4+d)$D problem, in order to describe its dimension.

2. Problem statement

2.1. Strong formulation

Let us consider a transient thermo-elasto-plastic problem. Under weak coupling assumption, the transient heat transfer analysis can be carried out prior to the mechanical analysis, by solving the following governing equation

$$\rho C\frac{d\theta(\mathbf{X},t)}{dt}+\text{div }\mathbf{q}(\mathbf{X},t)=r(\mathbf{X},t)\quad\text{in the matrial domain }\Omega \tag{1}$$

where "div •" is the divergence operator with respect to the initial position $\mathbf{X}$, d•/dt the material time derivative, ρ and C are respectively the material density and specific heat capacity, and r is the internal heat generation.

The linear isotropic Fourier constitutive law is enforced here

$$\mathbf{q}(\mathbf{X},t)=-\mathbf{k}.\nabla\theta(\mathbf{X},t) \tag{2}$$

where $\mathbf{k}$ is the thermal conductivity.

Different boundary conditions (BCs) and initial conditions can be defined

$$\begin{cases}\mathbf{q}(\mathbf{X},t).\mathbf{n}(\mathbf{X},t)=\overline{\mathbf{q}}(\mathbf{X},t) & \text{on the surface }\partial\Omega^{\mathbf{q}}\\ \theta(\mathbf{X},t)=\overline{\theta}(\mathbf{X},t) & \text{on the surface }\partial\Omega^{\theta}\\ \theta(\mathbf{X},t=0)=0\end{cases} \tag{3}$$

Considering a reference frame $\widetilde{\Omega}$ moving at constant velocity $\mathbf{v}$, the original problem reads

$$\rho C\frac{\partial\theta(\mathbf{x},t)}{\partial t}+\mathbf{div}\ \mathbf{q}(\mathbf{x},t)+\rho C\mathbf{v}.\nabla\theta(\mathbf{x},t)=r(\mathbf{x},t)\quad\mathbf{in}\ \widetilde{\Omega} \tag{4}$$

or with the steady-state assumption, as proposed in Ref. [17]

$$\text{div }\mathbf{q}(\mathbf{x},t)+\rho C\mathbf{v}.\nabla\theta(\mathbf{x},t)=r(\mathbf{x},t)\quad\text{in }\widetilde{\Omega}\quad\text{with}\ \frac{\partial\theta(\mathbf{x},t)}{\partial t}=0 \tag{5}$$

where $\mathbf{x}$ is the current position vector of a material point defined by $\mathbf{X}$ at initial time in $\widetilde{\Omega}$. At each time t, $\mathbf{x}=\mathbf{X}+\mathbf{v}t$. Note that the steady-state

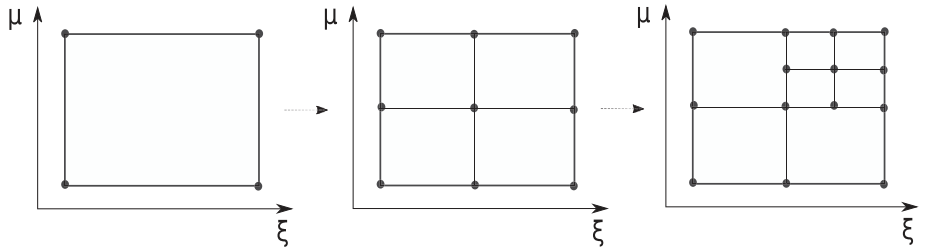

Fig. 2. Successive refinements in the 2D parameter space.

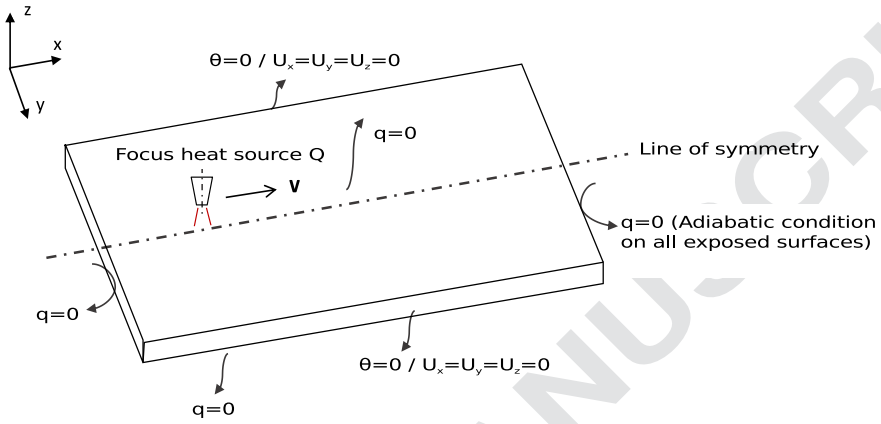

Fig. 3. Welding work-piece: geometry and boundary conditions.

Table 3
Material properties and load data.

Notation	Name	Values
C_p	Specific heat capacity	432 J kg^{-1} K^{-1}
λ	Thermal conductivity	46 W m^{-1} K^{-1}
α	Thermal expansion	1.2×10^{-5} K^{-1}
E	Young's modulus	210×10^{9} Pa
ν	Poisson ratio	0.3
σ_y	Initial yield stress	300×10^{6} Pa
H	Linear isotropic hardening parameter	21×10^{9} Pa
Q	Heat flux	8×10^{6} W m^{-2}
V	Velocity of loading	0.001 m s^{-1}

description is suitable for problems with a stationary regime reached throughout the process, like welding (e.g Refs. [40–42]). In addition, the solutions are solved in $\widetilde{\Omega}$, where BCs are not defined and should be chosen in an appropriate way to well approximate original solutions in the fixed frame. In this work, one adopts this steady-state formula for the thermal analysis in the moving frame.

Mechanical analysis is carried out in the fixed frame, which consists in seeking the admissible fields $\boldsymbol{\sigma}$, $\mathbf{u}$ and $\boldsymbol{\varepsilon}_p$ satisfying the following balance equations and BCs

$$\begin{cases} \operatorname{div}\boldsymbol{\sigma}(\mathbf{X},t)+\mathbf{f}(\mathbf{X},t)=0 & \text{in } \Omega \\ \boldsymbol{\sigma}(\mathbf{X},t).\mathbf{n}(\mathbf{X},t)=\overline{\mathbf{F}}(\mathbf{X},t) & \text{on } \partial\Omega^{\mathbf{F}} \\ \mathbf{u}(\mathbf{X},t)=\overline{\mathbf{u}}(\mathbf{X},t) & \text{on } \partial\Omega^{\mathbf{u}} \end{cases} \tag{6}$$

where $\boldsymbol{\sigma}=\mathbf{D}:\boldsymbol{\varepsilon}_e=\mathbf{D}:(\boldsymbol{\varepsilon}-\boldsymbol{\varepsilon}_p-\boldsymbol{\varepsilon}_\theta)$ with $\boldsymbol{\varepsilon}=\nabla_s\mathbf{u}(\mathbf{X},t)$, under infinitesimal strain assumption, and $\mathbf{D}$ denotes the fourth order elasticity tensor. The thermal strain denoted by $\boldsymbol{\varepsilon}_\theta$ results from the thermal expansion: $\boldsymbol{\varepsilon}_\theta=\alpha\theta\mathbf{I}$, where $\mathbf{I}$ is the second-order identity tensor and α is the thermal expansion coefficient.

The complementary plastic behavior law with an isotropic hardening R reads

$$\begin{cases} f(\boldsymbol{\sigma},\mathrm{p})=\|\boldsymbol{\sigma}_d\|-\sigma_y-\mathrm{R}(\mathrm{p}) \\ \dot{\varepsilon}_p=\mathcal{H}(f)\dfrac{<\boldsymbol{\sigma}_d:\dot{\boldsymbol{\sigma}}_d>}{\mathrm{R}_g}\dfrac{\boldsymbol{\sigma}_d}{\|\boldsymbol{\sigma}_d\|} \end{cases} \tag{7}$$

where σ_y denotes the initial yield stress, $\mathcal{H}(\bullet)$ the Heaviside function, $\boldsymbol{\sigma}_d$ the deviatoric stress tensor, $<A>$ the positive part of A, and p the equivalent plastic strains and $g=\frac{d\mathrm{R}}{d\mathrm{p}}$.

Then, the state vector of the thermo-elasto-plastic problem can be defined as

$$\mathbb{X}=\left\{\theta,\mathbf{u},\boldsymbol{\varepsilon}_p,\boldsymbol{\sigma},\mathrm{p}\right\}^T \tag{8}$$

2.2. Weak form and FE discretization

The variational formulation of the thermal problem (5) reads

$$\int_{\widetilde{\Omega}}\rho C\mathbf{v}.\nabla\theta\theta^*d\widetilde{\Omega}+\int_{\widetilde{\Omega}}\nabla\theta.\mathbf{k}.\nabla\theta^*d\widetilde{\Omega}+\int_{\partial\widetilde{\Omega}^{\mathbf{q}}}\overline{\mathbf{q}}\theta^*ds=\int_{\widetilde{\Omega}}r\theta^*d\widetilde{\Omega} \tag{9}$$

where θ and θ^* are respectively the trial and test functions.

With similar definitions for displacement functions $\mathbf{u}$ and $\mathbf{u}^*$, the equivalent mechanical variational form of (6) reads

$$-\int_\Omega\boldsymbol{\sigma}(\mathbf{u}):\varepsilon(\mathbf{u}^*)d\Omega+\int_\Omega\mathbf{f}.\mathbf{u}^*d\Omega+\int_{\partial\Omega^{\mathbf{F}}}\overline{\mathbf{F}}.\mathbf{u}^*ds=0 \tag{10}$$

The FE semi-discretized form for the thermo-elasto-plastic problem involves

$$\widetilde{\mathbf{K}}_{th}\boldsymbol{\theta}(t)=\mathbf{Q}(t) \tag{11}$$

where $\boldsymbol{\theta}$ and $\mathbf{Q}$ are respectively nodal temperature and external heat flux vector. The modified thermal conductivity matrix involves an additive advection term: $\widetilde{\mathbf{K}}_{th}=\sum_{elements}(\mathbf{B}_{th}^T.\mathbf{k}.\mathbf{B}_{th}+\mathbf{N}^T.\rho C\mathbf{v}^T.\mathbf{B}_{th})$, where $\mathbf{B}_{th}$

and $\mathbf{N}$ are the usual matrices respectively for temperature gradient and interpolation of the element temperature θ.

The mechanical solution is given when the following residual vanishes

$$\begin{cases} \mathbf{R}(\mathbf{U}(t)) = \mathbf{F}_{ext}(\mathbf{U}(t)) - \mathbf{F}_{int}(\mathbf{U}(t)) \\ \text{with} \quad \mathbf{F}_{ext}(t) = \displaystyle\int_{\Omega} \mathbf{N}^T.\mathbf{f}\, d\Omega + \int_{\partial\Omega^{\mathbf{F}}} \mathbf{N}^T.\overline{\mathbf{F}}\, ds \\ \mathbf{F}_{int}(t) = \displaystyle\int_{\Omega} \mathbf{B}_m^T.\boldsymbol{\sigma}\, d\Omega \end{cases} \tag{12}$$

where $\mathbf{U}$ is the nodal displacement vector, $\mathbf{F}_{ext}$ and $\mathbf{F}_{int}$ are respectively the associated external and internal force vectors. $\mathbf{B}_m$ is the usual matrix for displacement gradient.

Furthermore, this residual problem can be solved with the Newton-Raphson scheme and incorporated with the radial return mapping algorithm for plasticity flows. The transient thermal problem is solved by a first order time integrator.

3. A new strategy for multiparametric *computational vademecum*

This section presents a strategy for multidimensional parametric studies, based on the high order PGD (HOPGD) [36] which can be seen as an *a posteriori* version of standard PGD methods. A convergence acceleration technique, i.e. Aitken's Delta Squared method, is introduced to accelerate the convergence of this PGD construction. Furthermore, the multigrid snapshots selection is used to sample the parameter space.

3.1. A posteriori high order PGD-projection

Similarly to higher-order SVD or the PARAFAC methods, the HOPGD is proposed to obtain separated approximations of known functions. Given a d-dimensional function $f(\mu, \dots, \mu_d) \in L_2(\Omega)$ with coordinates $\mu_i|_{i=1,d}$, the HOPGD seeks a L_2 projection of the original function in the following form

$$\begin{aligned} f(\mu_1, \mu_2, \dots, \mu_d) &\approx f^n(\mu_1, \mu_2, \dots, \mu_d) \\ &= \sum_{m=1}^{n} F_1^m(\mu_1) F_2^m(\mu_2) \cdots F_d^m(\mu_d) \\ &= f^{n-1} + F_1^n(\mu_1) F_2^n(\mu_2) \cdots F_d^n(\mu_d) \end{aligned} \tag{13}$$

where n is the rank of approximation, $F_i^m|_{i=1,d}$ are the unknown functions of the m-th mode.

The L_2 projection is formulated as a minimization problem as follows

$$\begin{cases} \text{Find } f^n \in V_n \subset L_2(\Omega) \text{ such that} \\ J(f^n) = \min\limits_{f^n} \left(\dfrac{1}{2} \|f^n - f\|^2_{L_2(\Omega)} \right) \end{cases} \tag{14}$$

or equivalently the solution of

$$(f^n, f^s) = (f, f^s) \quad \text{for all } f^s \in V_n \tag{15}$$

The minimization problem can be solved by a greedy algorithm with an alternating direction strategy (fixed point iteration), as for PGD [21,43]. At each iteration n, the following local optimization problem is solved

$$\left(\prod_{i=1}^{d} F_d, \delta f \right) = (f - f^{n-1}, \delta f) \tag{16}$$

with test functions $\delta f = \delta \prod_{i=1}^{d} F_i = \delta F_1 F_2 \dots F_d + F_1 \delta F_2 \dots F_d + \dots + F_1 F_2 \dots \delta F_d$.

The alternating direction strategy is used for computing the components F_i, as illustrated in Algorithm 1.

The rank of approximation n is determined by the given accuracy, which means that the greedy algorithm will not stop until the error indicator is satisfied: $\frac{\|f^n - f\|^2}{\|f\|^2} \leq \epsilon_f$.

Robustness and efficiency have been shown in standard PGD methods with this kind of algorithm [21,43]. For a moderate multidimensional matrix, the HOPGD can be obtained efficiently with Algorithm 1. Several examples can be found in Ref. [36]. Moreover, it can

Algorithm 1: Alternating fixed point iteration

Input : Original function: f

Approximate with $n-1$ modes: f^{n-1}

Output: $F_i^n|_{i=1,d}$

while $\epsilon_i > \epsilon_c$ **do**
  $k \leftarrow k + 1$
  for $i \leftarrow 1$ **to** d **do**
    Assume all $F_{j\neq i}^{(k)}$ are fixed
    Compute $F_i^{(k)}$ by solving linearly (16)
  end
  Check convergence indicator $\epsilon_i = \frac{\|F_i^{(k)} - F_i^{(k-1)}\|^2}{\|F_i^{(k-1)}\|^2}$ for all $i \in [1, d]$
end
$F_i^n \leftarrow F_i^{(k)}|_{i=1,d}$
Return $F_i^n|_{i=1,d}$

be proved that in the case of two parameters, the HOPGD is equivalent to the well known SVD (POD method). For multi-parameters cases, the functions produced by HOPGD may not be optimal. Compared with HOSVD, HOPGD has the advantage of a straightforward generalization to high dimensions [36].

3.2. Convergence accelerator

One considers a convergent sequence $F_i^{(k)}$ in Algorithm 1. The equivalent fixed point formula reads

$$F_i^{(k+1)} = g(F_i^{(k)}) \tag{17}$$

The relaxation method can then be applied in order to accelerate the convergence of the resolution scheme. With a well chosen relaxation parameter w, the prediction of $\widetilde{F}_i^{(k+1)}$ at step k is improved by using the previous iterations without perturbing the stability of the numerical scheme

$$\begin{cases} \widetilde{F}_i^{(k+1)} = g(F_i^{(k)}) \\ F_i^{(k+1)} = w\widetilde{F}_i^{(k+1)} + (1-w)F_i^{(k)} \end{cases} \tag{18}$$

One possibility to compute w is given by Aitken's Delta Squared method [37,38], also called dynamic relaxation (the relaxation coefficient w is re-actualized at each iteration)

$$w^{(k)} = -w^{(k-1)}\frac{\delta_k}{\delta_{k+1} - \delta_k} \tag{19}$$

where $\delta_{k+1} = \widetilde{F}_i^{(k+1)} - F_i^{(k)}$. In the vector case, equation (19) reads

$$w^{(k)} = -w^{(k-1)}\frac{\boldsymbol{\delta}_k^T(\boldsymbol{\delta}_{k+1} - \boldsymbol{\delta}_k)}{\|\boldsymbol{\delta}_{k+1} - \boldsymbol{\delta}_k\|^2} \tag{20}$$

Remark 1. The relaxation parameter k is determined by taking into account two previous steps. Therefore, for the first two steps, there is no better guess for w except 1.

Remark 2. Application of this accelerator to the greedy algorithm 1 for HOPGD is straightforward. The relaxation parameter should be specific to each function $F_i|_{i=1,8}$ and re-actualized at every step. In vector cases, the relaxation parameter is calculated using equation (20) and applied for the concerned vector. This parameter estimation may be costly, but the speed-up for large dimensional cases is obvious, as shown hereinafter.

Considering a three dimensional matrix $\mathbf{U}(\mathbf{X}, t, \mu) \in \mathbb{R}^{9317\times117\times6}$, a FE solution of transient thermo-mechanical problems with a discretization of $9317 \times 117 \times 6$ respectively in space $\mathbf{X}$, time t and one material parameter μ, the HOPGD approximation is then given by

$$\mathbf{U}(\mathbf{X}, t, \mu) \approx \mathbf{U}^n(\mathbf{X}, t, \mu) = \sum_{m=1}^{n} \boldsymbol{\Phi}^m(\mathbf{X}) \otimes \mathbf{V}^m(t) \otimes \boldsymbol{F}^m(\mu) \tag{21}$$

where $\boldsymbol{\Phi}$ and $\mathbf{V}$ denote the space and time functions respectively. $\otimes$ is the usual tensor product operator.

The HOPGD coupled with the relaxation method shows a good convergence rate (see Fig. 1). Compared to the original fixed point sequence which convergents linearly, as shown in many cases [39], much fewer iterations are required in order to build the PGD functions when coupling with the relaxation process, and computational cost is much cheaper (Table 1).

Another comparison example for a higher dimensional matrix $\mathbf{U}(\mathbf{X}, t, \mu, \xi, \eta)$ is illustrated in Table 2. The discretization used for $\mathbf{X}, t, \mu, \xi$ and η is $9317 \times 117 \times 2 \times 2 \times 2$. The 5D HOPGD approximation reads then

$$\begin{aligned} \mathbf{U}(\mathbf{X}, t, \mu, \xi, \eta) &\approx \mathbf{U}^n(\mathbf{X}, t, \mu, \xi, \eta) \\ &= \sum_{m=1}^{n} \boldsymbol{\Phi}^m(\mathbf{X}) \otimes \mathbf{V}^m(t) \otimes \boldsymbol{F}_1^m(\mu) \otimes \boldsymbol{F}_2^m(\xi) \otimes \boldsymbol{F}_3^m(\eta) \end{aligned} \tag{22}$$

A good speed-up (almost 2×) has been shown in both two examples with application of the relaxation method. Although the constructed PGD functions are slightly modified by the relaxation, a good convergence rate is obtained, even for high dimensional matrices.

3.3. Separated variable representation

The presented HOPGD opens possibilities to perform the parametric studies for high dimensional problems, with some previous knowledge of the solution. As soon as the parameter functions (e.g $\boldsymbol{F}(\mu)$) are constructed, all solutions with respect to the variation of the parameter μ in its range can be known.

Considering a transient nonlinear thermo-mechanical problem, the prior known solutions $\mathbf{U}(\mathbf{X}, t)$, corresponding to different parameter values $\mu_i \in [\mu_1, \mu_N]$, are pre-computed with full FE models. The PGD functions $\boldsymbol{F}^m(\mu)$ are then provided by the HOPGD projection according to an error criterion. Any new solution corresponding to a new value in

Algorithm 2: Local interpolation

Input : The set of the operating points in the parameter space $\{\mu_1, \ldots, \mu_n\}$

PGD functions of $\mathbf{U}(\mathbf{X}, t, \mu)$: $(\boldsymbol{\Phi}^m(\mathbf{X}), \mathbf{V}^m(t), \boldsymbol{F}^m(\mu))_{m=1,n}$

New parameter value $\mu \notin \{\mu_1, \ldots, \mu_N\}$

Output: New solution $\mathbf{U}(\mu)$

1 **if** $\mu \in [\mu_i, \mu_{i+1}]$ **then**

2 Interpolation of the parameter function $\boldsymbol{F}^m(\mu)$ with $\boldsymbol{F}^m(\mu_i)$ and $\boldsymbol{F}^m(\mu_{i+1}) \rightarrow$ typical Lagrange interpolation for all $m \in [1, n]$

3 **end**

4 New solution $\mathbf{U}(\mu) = \sum_{m=1}^{n} \boldsymbol{\Phi}^m(\mathbf{X}) \otimes \mathbf{V}^m(t) \otimes \boldsymbol{F}^m(\mu)$

$[\mu_1, \mu_N]$ can be obtained with the local interpolation strategy illustrated in Algorithm 2.

Remark 3. A global interpolation can be chosen if necessary. Here, the parameter function is interpolated locally for the stabilization of schema.

3.4. Multigrid selection of the snapshots

The new solutions depend strongly on the quality of the basis functions constructed with snapshots. With the aim of selecting the snapshots that provide reliable solutions in the parameter space, a local

Algorithm 3: Local error indicator

Result: Local error indicator

Input : Domain $\mathcal{D}$

Output: Local error indicator ϵ

1 PGD functions of $\mathbf{U}(\mathbf{X}, t, \mu, \xi)$: $(\mathbf{\Phi}^m(\mathbf{X}), \mathbf{V}^m(t), \boldsymbol{F}_1^m(\mu), \boldsymbol{F}_2^m(\xi))_{m=1,n}$

2 $\mu_c, \xi_c \leftarrow$ the center of $\mathcal{D}$

3 Compute the HFM solution $\mathbf{U}_{\text{HFM}}(\mu_c)$ by full FEM

4 New solution $\mathbf{U}_{\text{HOPGD}} = \sum_{m=1}^{n} \mathbf{\Phi}^m(\mathbf{X}) \otimes \mathbf{V}^m(t) \otimes \boldsymbol{F}_1^m(\mu_c) \otimes \boldsymbol{F}_2^m(\xi_c)$ (Algorithm 2)

5 RB error $\epsilon(\mathbf{U}) = \frac{\|\mathbf{U}_{\text{HOPGD}}(t_m) - \mathbf{U}_{\text{HFM}}(t_m)\|_2}{\|\mathbf{U}_{\text{HFM}}(t_m)\|_2}$ (Eq. (23))

6 Return ϵ

Algorithm 4: Localized refinement of a 2D parameter space

Result: Localized refinement in a 2D parameter space

Input : Coarse first order grid $\mathcal{D}$ (square)
Tolerance ϵ_c

Output: $\mathcal{S}'$: list of the selected snapshots defining the localized refinement in the parameter space

1 $\mathcal{S} \leftarrow$ empty list

2 Check the corners of the current localized grid: $corn(\mathcal{D})$

3 Compute the error indicator ϵ (Algorithm 3)

4 **if** $\epsilon > \epsilon_c$ **then**

5 $\quad \mathcal{S}' \leftarrow \mathcal{S} \cup corn(\mathcal{D})$

6 $\quad$ Subdivide $\mathcal{D}$ into 4 subdomains (squares): $\mathcal{D}_{i=1,4}$

7 $\quad$ **for** $\mathcal{D}_i \in \{\mathcal{D}_1, \mathcal{D}_2, \mathcal{D}_3, \mathcal{D}_4\}$ **do**

8 $\quad\quad \mathcal{D} \leftarrow \mathcal{D}_i$

9 $\quad\quad$ go to line 2 and restart the recursive process

10 $\quad$ **end**

11 **else**

12 $\quad \mathcal{S}' \leftarrow \mathcal{S} \cup corn(\mathcal{D})$

13 **end**

14 Return $\mathcal{S}'$

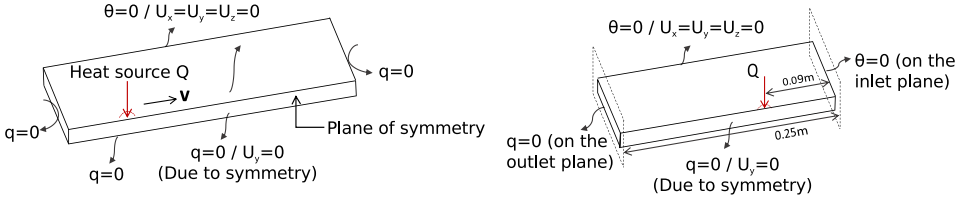

(a) Half model (b) Control volume

Fig. 4. Problem definition with boundary conditions.

Table 4
Geometry parameter of FE model.

L_x(m)	L_y(m)	L_z(m)	E.T.	E.N.	N.N.	G.N.
0.3	0.1	0.02	CUB8 (P1)	7200	9317	8

Notes. "E.T.": Element Type, "E.N." Element Number, "N.N.": Node Number, "G.N.": Gauss point Number per element.

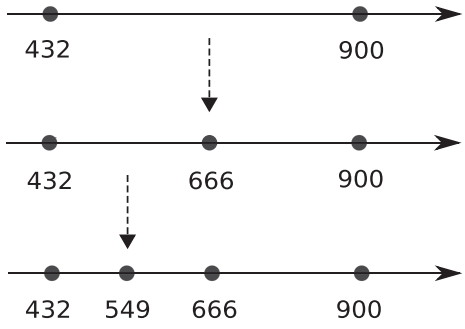

Fig. 5. Localized refinements in the 1D parameter space.

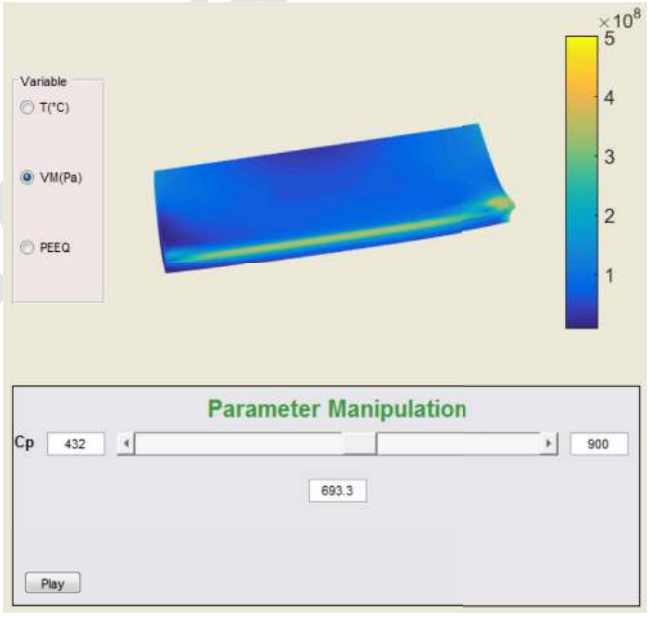

Fig. 6. 4 + 1D *computational vademecum* developed in matlab.

error control strategy is used.

Given a 2D parameter space $D : D_\mu \times D_\xi$ with $\mu \in D_\mu$ and $\xi \in D_\xi$, the location of snapshots that should be selected for constructing the reliable HOPGD functions can be determined through a local refinement approach which can be summarized into two main steps.

First of all, an error indicator should be defined for quantities of interest in order to assess the quality of grids. An example reads

$$\epsilon(\mathbf{U}) = \frac{\|\mathbf{U}_{\text{HOPGD}}(t_m) - \mathbf{U}_{\text{HFM}}(t_m)\|_2}{\|\mathbf{U}_{\text{HFM}}(t_m)\|_2} \tag{23}$$

where $(\bullet)(t_m)$ denotes the solution at the final time step and X_{HFM} the solution computed with high-fidelity model (HFM). The new solution $\mathbf{U}_{\text{HOPGD}}$ is computed at the center of the parameter space (see Algorithm 3). Although other choices of error indicator exist. This error, regarding the final quantities, is adopted since in welding problems the quantities of interest are usually those in final time, like residual stresses or welding induced distortions.

Then, the first order grid is defined as the corners of D. By subdividing the current domain, the refinement is successively executed when the error indicator is superior to the tolerance ϵ_c, which is illustrated in Algorithm 4.

An example of local refinements in the 2D parameter space is shown in Fig. 2. It should be noticed that the refinement is performed locally on the sub-domains where the error condition is not satisfied. Exhaus-

Table 5
Illustration of parameter refinement.

Grid order	Corners of the grid	Operating point	Error (σ_{VM})	Error test
1	432, 900	666	4.75%	0
2	432, 666	549	1.85%	0
2	666, 900	783	1.15%	1
3	432, 549	490.5	0.90%	1
3	549, 666	607.5	0.82%	1
3	666, 900	724.5	1.15%	1

Notes. "Error test: 1/0" means the error condition is satisfied or not.

Table 6
CPU time and memory for 4 + 1D *computational vademecum*.

	Offline			Online
	4 snapshots	HOPGD	Total	
CPU time	28 h	1200 s	< 29 h	< 1 s
Memory	166 Mbytes	40 Mbytes	40 Mbytes	–
Full FEM	–	–	–	7 h

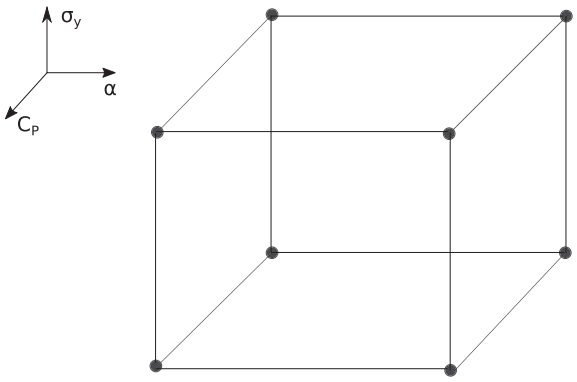

Fig. 7. 3D parameter space with snapshots.

tive generations of snapshots in the parameter space can therefore be avoided. And the error of the final grid is controllable.

Similar adaptive sampling strategies have been used in RB methods [44–46] (see also an adaptation to PGD [47]). In those methods, the sampling points for constructing the RB are selected and enriched through a greedy algorithm coupled with a residue analysis dedicated to estimate the error of each sub-domain, at offline stage. The refinement effort is then localized on those domains where the error condition is not satisfied. Compared to these methods, the proposed method may involve more HFM computations, since the evaluation of the error estimate requires expensive standard full computations. This point requires to be improved by considering another inexpensive error estimator for the proposed method (e.g *a posteriori* residue analysis in the parameter space).

4. Application examples: *computational vademecum of welding*-like simulations

4.1. Numerical model

The work-piece with prescribed boundary conditions is shown in Fig. 3. The heat source moves along the line of symmetry. The used material properties as well as the load parameters are given in Table 3. All the material properties are assumed independent on the temperature.

Since the problem (geometry, material, loading, BCs) is x-z plane symmetric, only one half of the actual problem is modeled Fig. 4(a). The mesh characteristics are presented in Table 4.

The thermal analysis is performed in the moving frame for a good efficiency. The control volume is defined as a domain of 0.25 m long (see Fig. 4(b)), in which the material flows through with the same constant velocity as loading in the x direction. The laser can be therefore viewed as a fixed loading in the control volume and is located 0.09 m from the inlet boundary. The inlet boundary is prescribed with the initial temperature $\theta_0 = 0$, while the outlet boundary is prescribed with zero heat flux.

One recalls here the state vector of the problem

$$\mathbb{X} = \left\{\theta, \mathbf{u}, \boldsymbol{\varepsilon}_p, \boldsymbol{\sigma}, \mathrm{p}\right\}^T \tag{24}$$

4.2. 4 + 1D computational vademecum

Let us consider a material parameter C_p(J kg^{-1} K^{-1}) ranging in [432 900], in order to study its influence on the quantities of interest of the welding problem (e.g. residual stresses and distortions), parametric solutions are required. The HOPGD representation reads then

$$\mathbf{U}(\mathbf{X}, t, C_p) \approx \sum_{m=1}^{n} \boldsymbol{\Phi}^m(\mathbf{X}) \otimes \mathbf{V}^m(t) \otimes \boldsymbol{F}^m(C_p) \tag{25}$$

For the sake of computing the basis functions that can provide accurate solutions (error <1.5%), 4 snapshots {432 549 666 900} are selected in the parameter range with the multigrid selection method, after two localized refinements, as shown in Fig. 5. The errors of residual stress corresponding to each order of grid can be found in Table 5. The same work can be done for other state variables. These 4D parametric solutions form then a *computational vademecum* (see Fig. 6). Moreover, as it is shown in Table 6, the memory needed for storing the HOPGD functions is very limited (<40 Mbytes) and the *computational vademecum* can provide real-time solutions, whereas it takes 7 h for

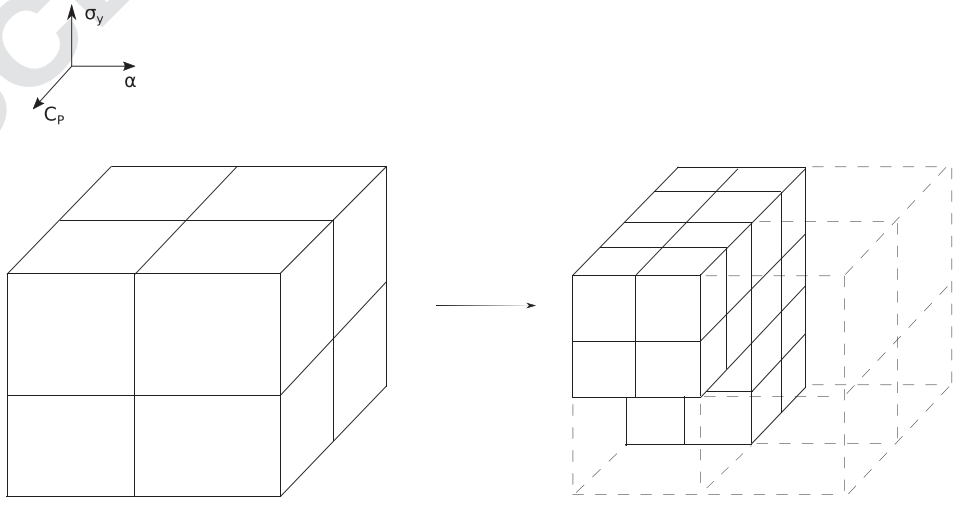

Fig. 8. Successive local refinements in the 3D parameter space.

Table 7
Errors at some operating points in the refined 3D parameter space.

Grid order	Operating point (C_p, α, σ_y)	Error (σ_{VM})	Error (p)
3	(783 1.215 350)	3%	5%
3	(549 1.485 450)	3%	6%
3	(490.5 1.1475 375)	1%	3%
3	(607.5 1.2825 325)	1%	2%
3	(490.5 1.1475 475)	1%	3%
3	(607.5 1.2825 425)	1%	2%
3	(724.5 1.1475 475)	1%	3%
3	(841.5 1.2825 425)	1%	2%

running a complete FE calculation and needs more than 160 Mbytes to store the complete FE solutions.

Similar results can be found in the work of [34] using a POD-based approach. In that case, the memory required for storing the snapshots is less than here, since the POD basis functions are optimal. However, for multiparameter cases, the POD-based approach becomes less efficient.

4.3. 4 + 3D computational vademecum

This section presents an example of 4 + 3D *computational vademecum* taking into account three material parameters: thermal capacity C_p(J kg^{-1} K^{-1}) $\in \mathcal{D}_C = [432\ 900]$, thermal expansion $\alpha(10^{-5}\ \mathrm{K}^{-1}) \in \mathcal{D}_\alpha = [1.08\ 1.62]$ and initial yield stress σ_y(MPa) $\in \mathcal{D}_\sigma = [300\ 500]$. In this case, the HOPGD representation of the solution of the welding problem reads

$$\mathbf{U}(\mathbf{X}, t, C_p, \alpha, \sigma_y) \approx \sum_{m=1}^{n} \mathbf{\Phi}^m(\mathbf{X}) \otimes \mathbf{V}^m(t) \otimes \boldsymbol{F}_1^m(C_p) \otimes \boldsymbol{F}_2^m(\alpha) \otimes \boldsymbol{F}_3^m(\sigma_y) \quad (26)$$

The parameter space $\mathcal{D} \coloneqq \mathcal{D}_C \times \mathcal{D}_\alpha \times \mathcal{D}_\sigma$ and the 8 snapshots defining the first order grid are illustrated in Fig. 7. In order to have reliable solutions (with error $\lesssim 6\%$), two successive localized refinements with the multigrid method are performed in the 3D parameter space (see Fig. 8). The solution errors associated with some operating points are shown in Table 7. As shown in Fig. 9, the snapshots needed for providing accurate thermo-mechanical solutions with HOPGD are localized in some sub-domains of the 3D parameter space.

The memory storage and the total offline CPU time (including snapshots computations and HOPGD) for constructing this *computational vademecum* (see Fig. 10) is shown in Table 8. On the one hand, HOPGD approximation allows an economic storage of snapshots (full FE solutions which require 3Gbytes totally). On the other hand, instead of running FE computation which takes 7h for a new parameter value, the space-time solutions for new parameters can be provided at real time rates (<1s) by the *computational vademecum*. Although the offline cost for building the snapshots and HOPGD may be expensive (which should be much less with parallel solvers), it is obviously advantageous to loose time at this stage compared to that earned at online phase, especially in the case of repetitive tasks.

Other process parameters can be also taken into account for building the *computational vademecum*. This kind of *computational vademecum* can serve as a database and be used online by engineers for optimization or inverse identification problems of welding processes.

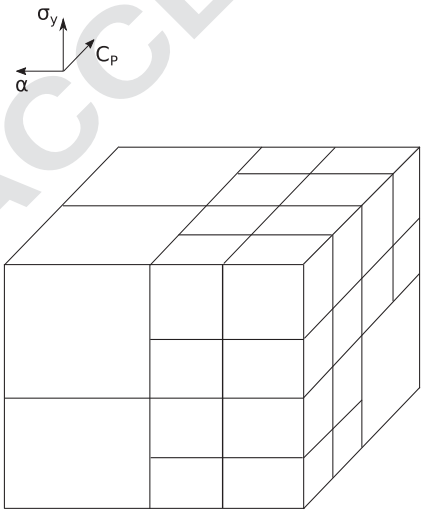

Fig. 9. Final grid (order 3) in the 3D parameter space.

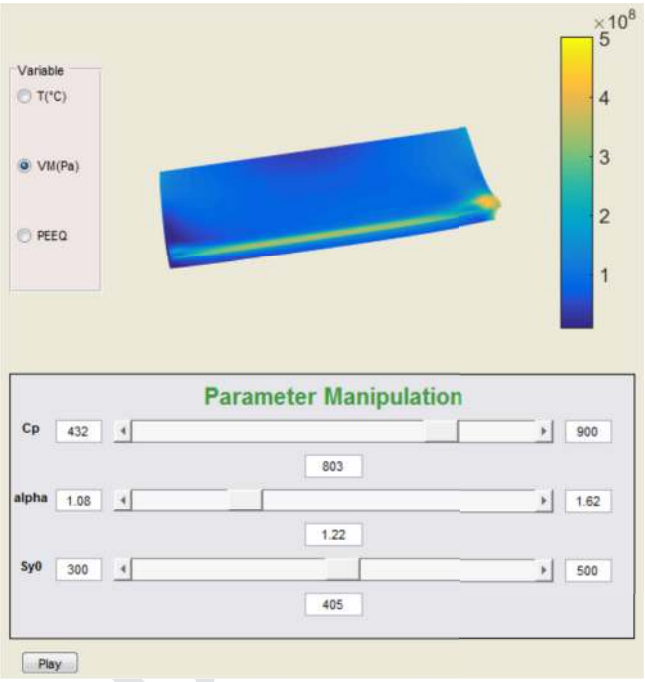

Fig. 10. 4 +3D *computational vademecum.*

Table 8
CPU time and memory for 4 + 3D *computational vademecum*.

	Offline			Online
	74 snapshots	HOPGD	Total	
CPU time	518 h	15 h	533 h	< 1 s
Memory	3 Gbyts	654 Mbyts	654 Mbyts	–
Full FEM	–	–	–	7 h

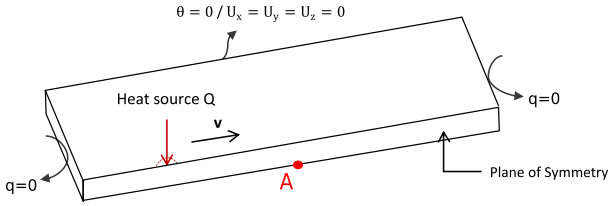

Fig. 11. Welding model and the position of the studied interest quantity: deflection in A.

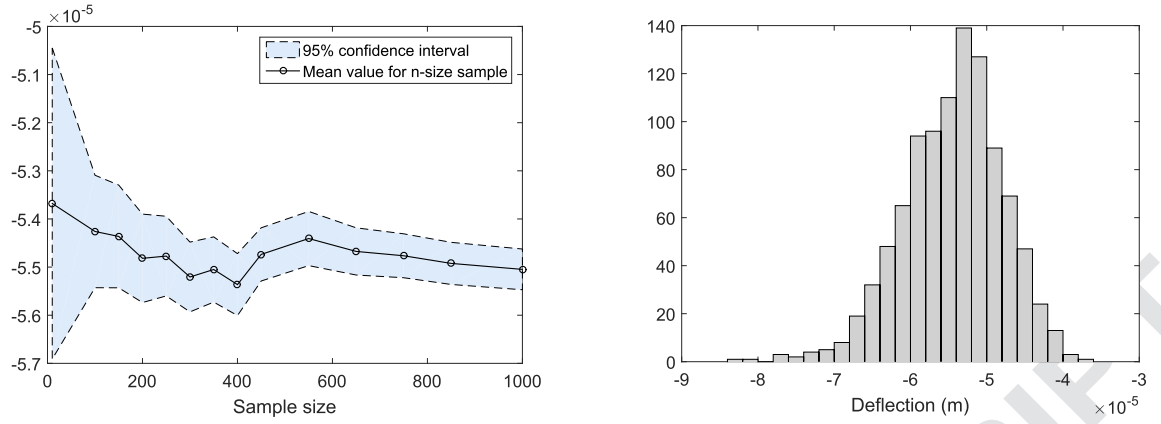

Fig. 12. Numerical experiences for sensitivity analysis.

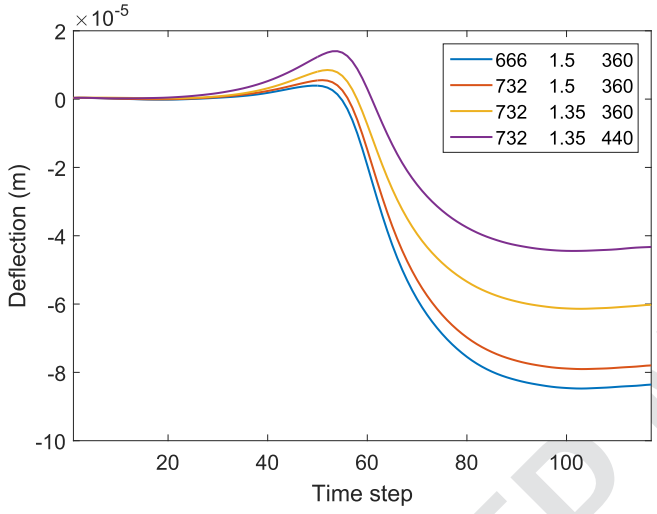

Fig. 13. Deflection of the welding work-piece modified by three input parameters C_p, α, σ_y.

4.4. Application of computational vademecum to sensitivity analysis

Sensitivity analysis consists in the study of the influence of input variation (uncertainties) on the output of a model. It is usually applied to numerical welding simulation in order to find out the dominant variables on the output quantities (e.g. distortions or residual stresses) [48].

This section illustrates the application of the constructed $4+3$D *computational vademecum* for sensitivity analysis. As an example, the influence of material parameters on the deflection of the welding work-piece is studied herein. The displacement of the point A located at the center of the bottom is selected as a measure of deflection (see Fig. 11). For different input parameters, the outputs (space-time simulations of welding) can be provided by the *computational vademecum* very fast, which makes possible a database with a large number of numerical experiences. Such an approach allows to avoid the cumbersome task of repeating huge computations with a sampling technique.

Let us assume a set of material properties with uncertainties on three parameters modeled as random variables with a normal distribution: thermal capacity $C_p(\mathrm{J\,kg^{-1}\,K^{-1}}) \sim \mathcal{N}(666, 66.6^2)$, thermal expansion $\alpha(10^{-5}\mathrm{K^{-1}}) \sim \mathcal{N}(1.35, 0.13^2)$ and initial yield stress $\sigma_y(\mathrm{MPa}) \sim \mathcal{N}(400, 40^2)$, where $\mathcal{N}(\overline{\mu}, \sigma^2)$ denotes the normal distribution with a mean $\overline{\mu}$ and a standard deviation σ. The convergence of the random sampling is reached with 6050 numerical experiences, as shown in Fig. 12(a). The mean value of the deflection is -5.48×10^{-5}m. It should be highly noticed that these 6050 experiences need totally 6050×7 h (5 years !) with standard FE simulations. With the constructed *computational vademecum*, the convergence is inexpensive, since the solutions can be generated at very low cost (<20 min). Fig. 12(b) illustrates the distribution of the work-piece deflections at final time with 1000 numerical experiences. It is shown that the distribution of outputs has a standard deviation of 12%, like input parameters. Focusing now on the time evolution of the deflection in A, one can see that the deflection is mainly influenced by α and σ_y and slightly modified by the variation of C_p, as shown in Fig. 13.

5. Conclusion

A new *a posteriori* non-intrusive strategy dedicated to construction of multiparametric *computational vademecum* has been presented. A separate representation of solutions, which contains explicitly the parameter functions allowing the exploitation of the parameter space, is constructed by the HOPGD method with some pre-computed snapshots. A dynamic relaxation method has been successfully applied to improve the convergence rate of the HOPGD procedure. In order to efficiently sample the parameter space, a multigrid method that allows automatic localized refinements is employed to select the snapshots.

The application to construct *computational vademecum* for a nonlinear thermo-mechanical problem shows the efficiency of the proposed approach. For a given level of accuracy, limited memory is necessary to store the snapshots. And the *computational vademecum* can provide real-time space-time online response for any parameter value. The use of *computational vademecum* can be helpful for simulation-based engineering and sensitivity analysis. Future work consists in applying the proposed approach to industrial engineering problems of welding (with more realistic loading and possible complex metallurgy effects) and the improvement of the multigrid method for high dimensional problems.

Acknowledgements

The authors gratefully acknowledge AREVA and SAFRAN for funding of this work within the framework of the “Life extension and manufacturing processes” teaching and research Chair.

References

[1] P. Holmes, J.L. Lumley, G. Berkooz, Turbulence, Coherent Structures, Dynamical Systems and Symmetry, Cambridge University Press, 1998.
[2] F. Chinesta, A. Leygue, F. Bordeu, J. Aguado, E. Cueto, D. González, I. Alfaro, A. Ammar, A. Huerta, Pgd-based computational vademecum for efficient design, optimization and control, Arch. Comput. Methods Eng. 20 (1) (2013) 31–59.
[3] M. Vitse, D. Néron, P.-A. Boucard, Virtual charts of solutions for parametrized nonlinear equations, Comput. Mech. 54 (6) (2014) 1529–1539.

[4] A. Courard, D. Néron, P. Ladeveze, P. Andolfatto, A. Bergerot, Virtual charts for shape optimization of structures, in: 2nd ECCOMAS Young Investigators Conference (YIC 2013), 2013.

[5] S. Niroomandi, I. Alfaro, E. Cueto, F. Chinesta, Model order reduction for hyperelastic materials, Int. J. Numer. Methods Eng. 81 (9) (2010) 1180–1206.

[6] K. Kunisch, S. Volkwein, Galerkin proper orthogonal decomposition methods for parabolic problems, Numer. Math. 90 (1) (2001) 117–148.

[7] J. Yvonnet, Q.-C. He, The reduced model multiscale method (r3m) for the non-linear homogenization of hyperelastic media at finite strains, J. Comput. Phys. 223 (1) (2007) 341–368.

[8] D. Amsallem, M.J. Zahr, C. Farhat, Nonlinear model order reduction based on local reduced-order bases, Int. J. Numer. Methods Eng. 92 (10) (2012) 891–916.

[9] D. Ryckelynck, Hyper-reduction of mechanical models involving internal variables, Int. J. Numer. Methods Eng. 77 (1) (2009) 75–89.

[10] K. Carlberg, C. Farhat, J. Cortial, D. Amsallem, The gnat method for nonlinear model reduction: effective implementation and application to computational fluid dynamics and turbulent flows, J. Comput. Phys. 242 (2013) 623–647.

[11] P. Kerfriden, P. Gosselet, S. Adhikari, S.P.-A. Bordas, Bridging proper orthogonal decomposition methods and augmented newton–krylov algorithms: an adaptive model order reduction for highly nonlinear mechanical problems, Comput. Methods Appl. Mech. Eng. 200 (5) (2011) 850–866.

[12] J. Hernández, J. Oliver, A.E. Huespe, M. Caicedo, J. Cante, High-performance model reduction techniques in computational multiscale homogenization, Comput. Methods Appl. Mech. Eng. 276 (2014) 149–189.

[13] A. Coriglianoa, M. Dossia, S. Mariania, Model Order Reduction and Domain Decomposition Strategies for the Solution of the Dynamic Elastic-plastic Structural Problem.

[14] M. Barrault, Y. Maday, N.C. Nguyen, A.T. Patera, An 'empirical interpolation'method: application to efficient reduced-basis discretization of partial differential equations, Comptes Rendus Math. 339 (9) (2004) 667–672.

[15] S. Chaturantabut, D.C. Sorensen, Nonlinear model reduction via discrete empirical interpolation, SIAM J. Sci. Comput. 32 (5) (2010) 2737–2764.

[16] D. Ryckelynck, A priori hyperreduction method: an adaptive approach, J. Comput. Phys. 202 (1) (2005) 346–366.

[17] Y. Zhang, A. Combescure, A. Gravouil, Efficient hyper reduced-order model (hrom) for parametric studies of the 3d thermo-elasto-plastic calculation, Finite Elem. Anal. Des. 102 (2015) 37–51.

[18] S. Niroomandi, I. Alfaro, E. Cueto, F. Chinesta, Real-time deformable models of non-linear tissues by model reduction techniques, Comput. Methods Programs Biomed. 91 (3) (2008) 223–231.

[19] S. Niroomandi, I. Alfaro, E. Cueto, F. Chinesta, Accounting for large deformations in real-time simulations of soft tissues based on reduced-order models, Comput. Methods Programs Biomed. 105 (1) (2012) 1–12.

[20] F. Chinesta, A. Ammar, E. Cueto, Recent advances and new challenges in the use of the proper generalized decomposition for solving multidimensional models, Arch. Comput. Methods Eng. 17 (4) (2010) 327–350.

[21] F. Chinesta, P. Ladeveze, E. Cueto, A short review on model order reduction based on proper generalized decomposition, Arch. Comput. Methods Eng. 18 (4) (2011) 395–404.

[22] F. Chinesta, E. Cueto, PGD-based Modeling of Materials, Structures and Processes, Springer, 2014.

[23] P. Ladevèze, Sur une famille d'algorithmes en mécanique des structures, in: Comptes rendus des séances de l'Académie des sciences. Série 2, Mécanique-physique, chimie, sciences de l'univers, sciences de la terre, 300(2), 1985, pp. 41–44.

[24] P. Ladeveze, J.-C. Passieux, D. Néron, The Latin multiscale computational method and the proper generalized decomposition, Comput. Methods Appl. Mech. Eng. 199 (21) (2010) 1287–1296.

[25] P. Ladevèze, Nonlinear Computational Structural Mechanics: New Approaches and Non-incremental Methods of Calculation, Springer Science & Business Media, 2012.

[26] A. Ammar, B. Mokdad, F. Chinesta, R. Keunings, A new family of solvers for some classes of multidimensional partial differential equations encountered in kinetic theory modeling of complex fluids, J. Newt. Fluid Mech. 139 (3) (2006) 153–176.

[27] A. Ammar, B. Mokdad, F. Chinesta, R. Keunings, A new family of solvers for some classes of multidimensional partial differential equations encountered in kinetic theory modelling of complex fluids: Part ii: transient simulation using space-time separated representations, J. Newt. Fluid Mech. 144 (2) (2007) 98–121.

[28] E. Nadal, F. Chinesta, P. Díez, F. Fuenmayor, F. Denia, Real time parameter identification and solution reconstruction from experimental data using the proper generalized decomposition, Comput. Methods Appl. Mech. Eng. 296 (2015) 113–128.

[29] J.V. Aguado, A. Huerta, F. Chinesta, E. Cueto, Real-time monitoring of thermal processes by reduced-order modeling, Int. J. Numer. Methods Eng. 102 (5) (2015) 991–1017.

[30] C. Ghnatios, F. Masson, A. Huerta, A. Leygue, E. Cueto, F. Chinesta, Proper generalized decomposition based dynamic data-driven control of thermal processes, Comput. Methods Appl. Mech. Eng. 213 (2012) 29–41.

[31] S. Niroomandi, D. González, I. Alfaro, F. Bordeu, A. Leygue, E. Cueto, F. Chinesta, Real-time simulation of biological soft tissues: a pgd approach, Int. J. Numer. Methods Biomed. Eng. 29 (5) (2013) 586–600.

[32] D. González, I. Alfaro, C. Quesada, E. Cueto, F. Chinesta, Computational vademecums for the real-time simulation of haptic collision between nonlinear solids, Comput. Methods Appl. Mech. Eng. 283 (2015) 210–223.

[33] C. Quesada, D. González, I. Alfaro, E. Cueto, F. Chinesta, Computational vademecums for real-time simulation of surgical cutting in haptic environments, Int. J. Numer. Methods Eng. 108 (10) (2016) 1230–1247.

[34] Y. Lu, N. Blal, A. Gravouil, Real time space-time pod based *computational vademecums* for parametric studies: application to thermo-mechanical problems, Adv. Model. Simul. Eng. Sci. 2017.

[35] D. Amsallem, C. Farhat, Interpolation method for adapting reduced-order models and application to aeroelasticity, AIAA J. 46 (7) (2008) 1803–1813.

[36] D. Modesto, S. Zlotnik, A. Huerta, Proper generalized decomposition for parameterized helmholtz problems in heterogeneous and unbounded domains: application to harbor agitation, Comput. Methods Appl. Mech. Eng. 295 (2015) 127–149.

[37] B.M. Irons, R.C. Tuck, A version of the aitken accelerator for computer iteration, Int. J. Numer. Methods Eng. 1 (3) (1969) 275–277.

[38] U. Küttler, W.A. Wall, Fixed-point fluid–structure interaction solvers with dynamic relaxation, Comput. Mech. 43 (1) (2008) 61–72.

[39] M. Duval, Apports du couplage non-intrusif en mécanique non-linéaire des structures, Ph.D. thesis, Université Paul Sabatier-Toulouse III, 2016.

[40] D. Balagangadhar, G. Dorai, D. Tortorelli, U. of Illinois at Urbana-Champaign, A displacement-based reference frame formulation for steady-state thermo-elasto-plastic material processes, Int. J. Solids Struct. 36 (16) (1999) 2397–2416.

[41] S.M. Rajadhyaksha, P. Michaleris, Optimization of thermal processes using an eulerian formulation and application in laser surface hardening, Int. J. Numer. Methods Eng. 47 (11) (2000) 1807–1823.

[42] D. Canales, A. LeygueF. Chinesta, D. González, E. Cueto, E. Feulvarch, J.-M. Bergheau, A. Huerta, Vademecum-based gfem (v-gfem): optimal enrichment for transient problems, Int. J. Numer. Methods Eng. 108 (9) (2016) 971–989.

[43] A. Nouy, A priori model reduction through proper generalized decomposition for solving time-dependent partial differential equations, Comput. Methods Appl. Mech. Eng. 199 (23) (2010) 1603–1626.

[44] A. T. Patera, An "hp" certified reduced basis method for parametrized elliptic partial differential equations, SIAM J. Sci. Comput. 32 3170–3200.

[45] B. Haasdonk, M. Dihlmann, M. Ohlberger, A training set and multiple bases generation approach for parameterized model reduction based on adaptive grids in parameter space, Math. Comput. Model. Dyn. Syst. 17 (4) (2011) 423–442.

[46] Y. Maday, B. Stamm, Locally adaptive greedy approximations for anisotropic parameter reduced basis spaces, SIAM J. Sci. Comput. 35 (6) (2013) A2417–A2441.

[47] C. Heyberger, P.-A. Boucard, D. Néron, A rational strategy for the resolution of parametrized problems in the pgd framework, Comput. Methods Appl. Mech. Eng. 259 (2013) 40–49.

[48] O. Asserin, A. Loredo, M. Petelet, B. Iooss, Global sensitivity analysis in welding simulations—what are the material data you really need?,, Finite Elem. Anal. Des. 47 (9) (2011) 1004–1016.